ONLINE SUPPLEMENT

An inducible hepatocellular carcinoma model for preclinical evaluation of anti-angiogenic therapy in adult mice

Anja Runge, Junhao Hu, Matthias Wieland, Jan-Philip Bergeest, Carolin Mogler,
André Neumann, Cyrill Géraud, Bernd Arnold, Karl Rohr,
Dorde Komljenovic, Peter Schirmacher, Sergij Goerdt, Hellmut G. Augustin

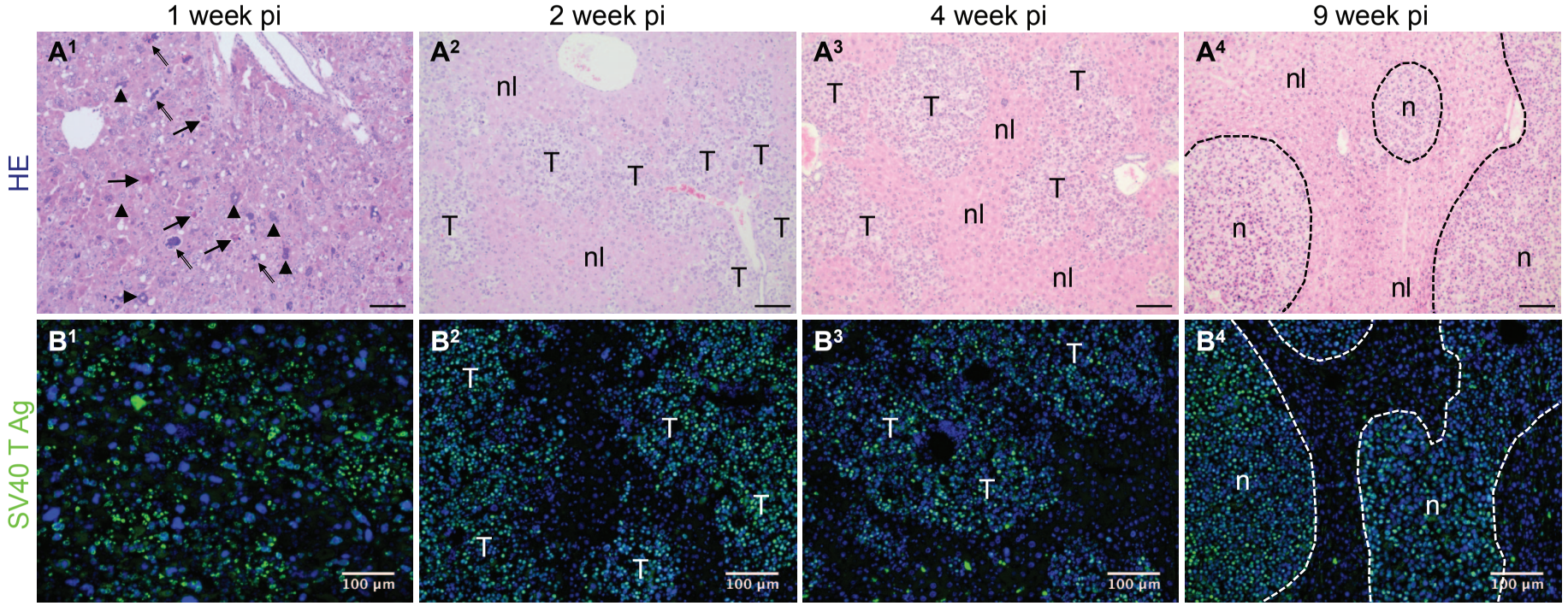

Supplementary Figure S1: Kinetics of tumorigenic transformation. Representative images of HE (A) and SV40 T Ag (B) stainings of paraffin-embedded and frozen liver sections. Acute viral hepatitis and parenchymal destruction developed at 1 week (A^1) post-adenovirus Cre infection (pi). Note, the appearance of giant cells (arrowheads), mitosis (thin arrows) and apoptosis (thick arrows). At 2 weeks pi (A^2), signs of acute hepatitis decreased and atypical hepatocytes appeared with a shifted nuclear-cytoplasmic ratio forming nodular structures at 4 weeks pi (A^3). Fully developed HCC was seen at 9 weeks pi (A^4, dashed line). Extensive SV40 T Ag expression appeared as early as 1 week pi (B^1) ubiquitously throughout the liver area, declining to the tumorous transformed regions at week 2 and 4 pi (B^2, B^3), which is further restricted to the tumor nodules at 9 weeks pi (B^4, dashed line). Scale bar HE: 50 µm, SV40 T Ag: 100 µm. nl, normal liver; T, tumorigenic area; n, nodules.

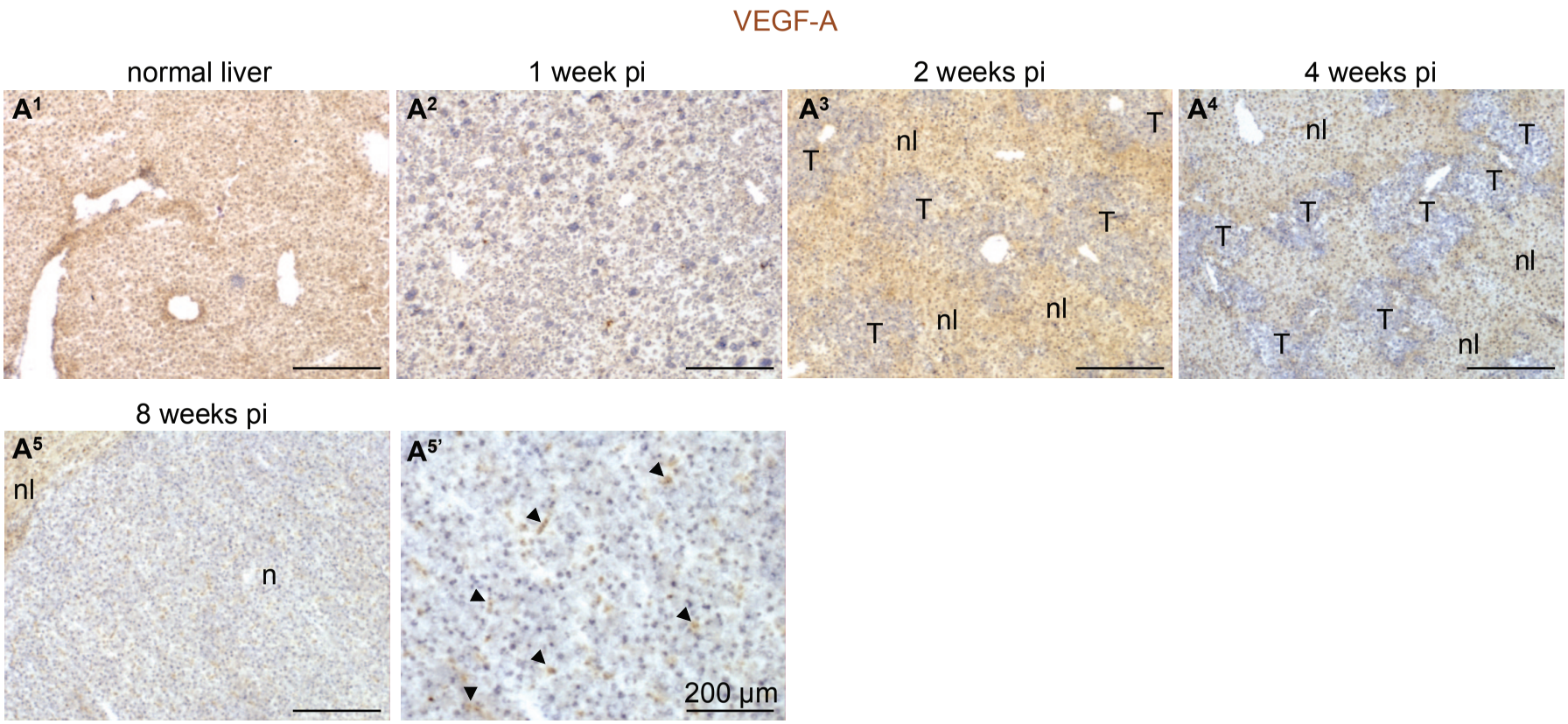

Supplementary Figure S2: Kinetics of VEGF-A expression. Representative images of VEGF-A staining of frozen liver sections. Normal liver represented a relative high baseline VEGF-A expression (A^1). During the early phase of tumorous transformation and acute viral hepatitis, 1 week post-adenvirus Cre infection (pi) , VEGF-A expression was downregulated (A^2). At 2 and 4 weeks pi (A^3, A^4) VEGF-A expression resumed to baseline levels in the regenerated hepatocytes, however, in the nodular structures VEGF-A was not upregulated, due to the micro vasculature (see CD31 staining in Fig. 2E, G, I). At 8 weeks pi (A^5) VEGF-A was occasionally upregulated within the nodular area in single cells (arrows in A^5, higher magnification). Scale bar: 500 µm; nl, normal liver; T, tumorigenic area; n, nodules.

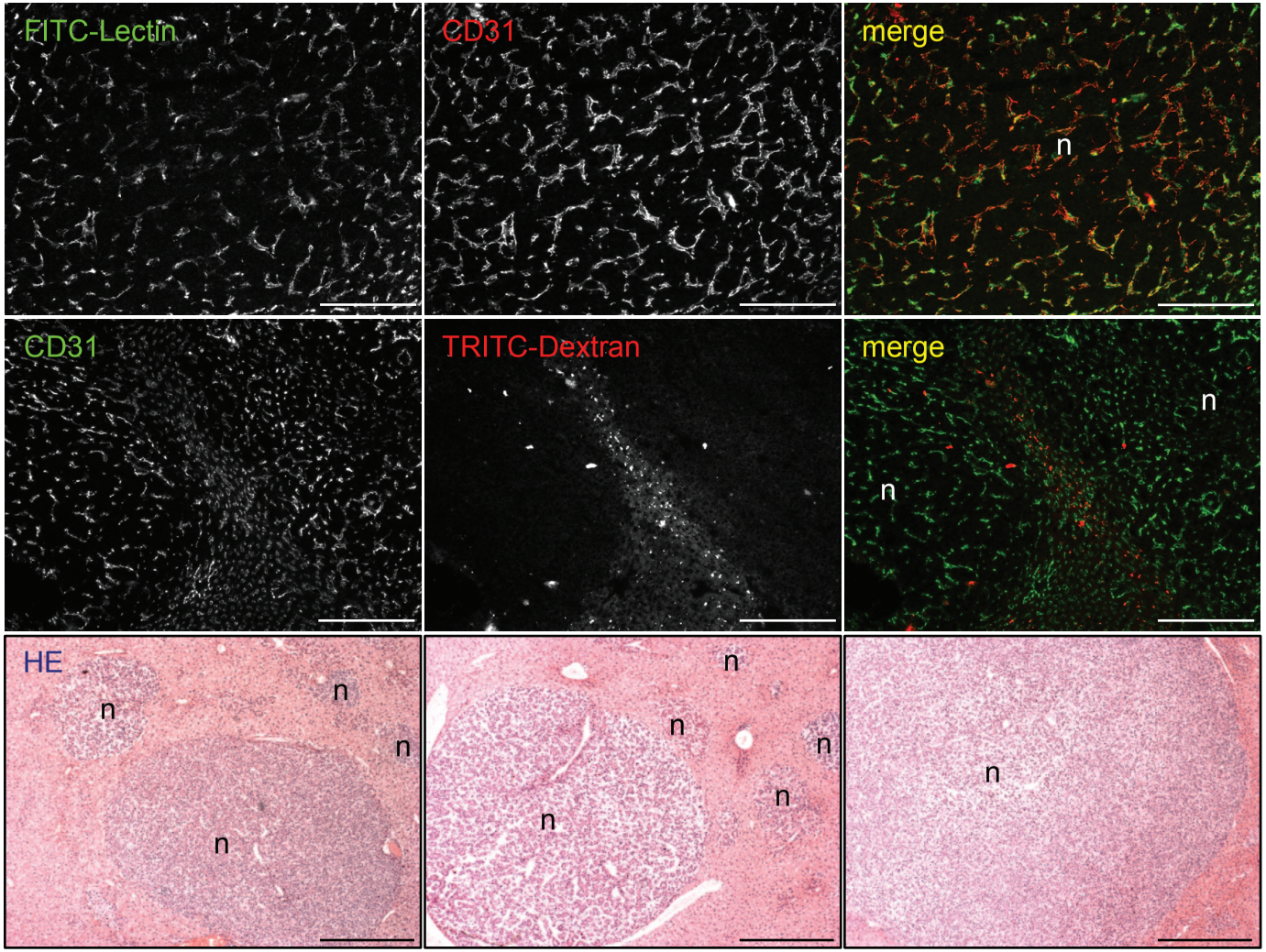

Supplementary Figure S3: Functional liver tumor vasculature. Images of frozen liver sections of Lectin-FITC perfused liver samples where further stained with CD31 (upper row), indicating perfusion of vessels in the tumor nodules. Low molecular weight TRITC-Dextran perfused liver samples where further stained with CD31 (middle row) demonstrating no vessel leakage in the tumor nodules; vascular leakage occured outside the nodular area as a characteristics of sinusoids. HE stained liver sections (lower row) showing different nodule size with no overt necrosis. Scale bar: 200 µm; n, nodules.

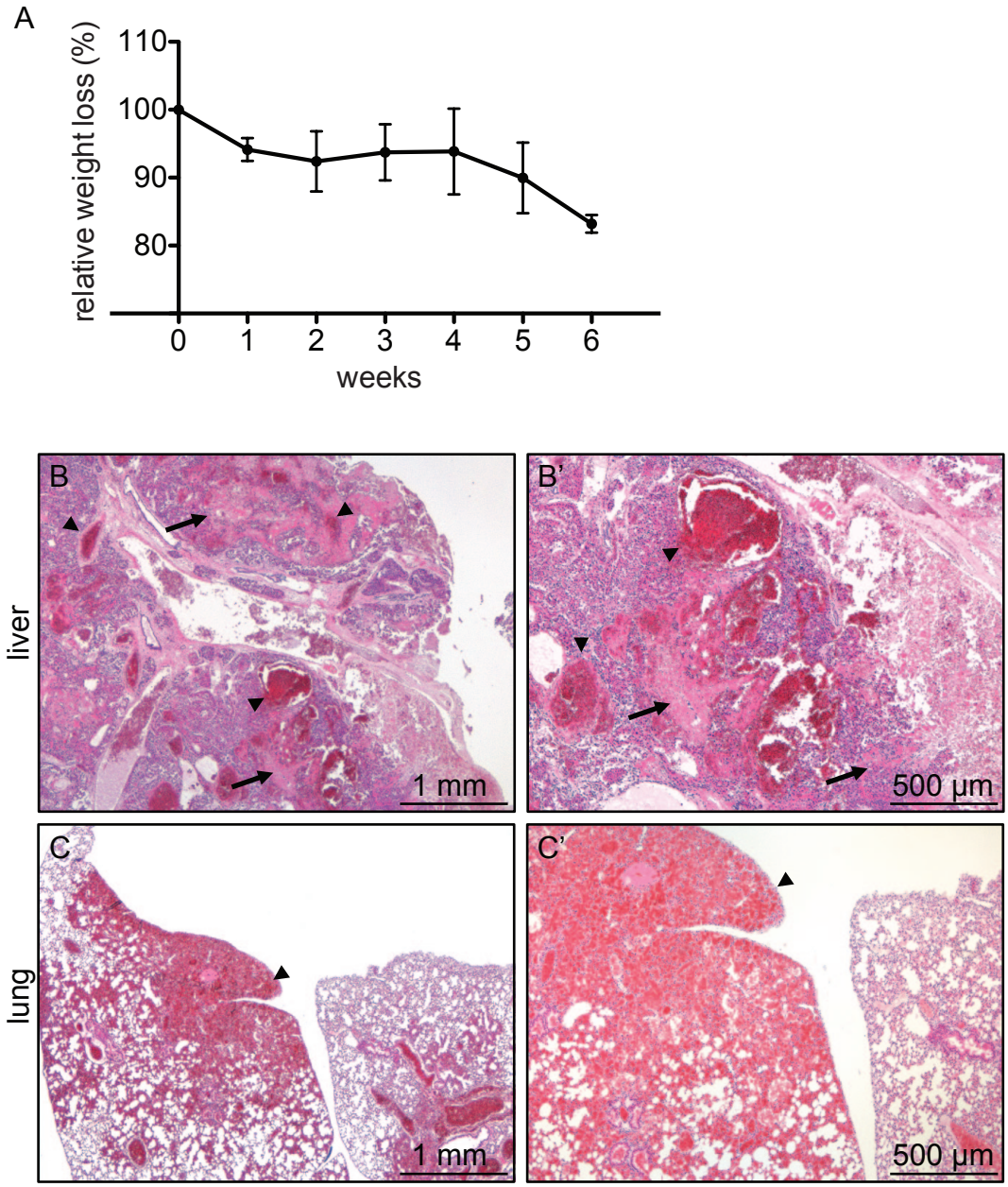

Supplementary Figure S4: Side effects in the long-term Sorafenib-treated iAST mice. Sorafenib-treated (60 mg/kg), MRI staged mice (here, late treatment initiation), indicated substantial weight loss over time (A). HE staining of paraffin-embedded liver and lung sections from adenovirus Cre recombinase injected iAST mice, treated long-term with Sorafenib. (B, C) Representative images of the liver and lung sections showing severe necrosis (arrows), hemorrhage and bleeding (arrowheads) in the heavily damaged liver (B, B‘ higher magnification) as well as lung bleeding (arrowhead) in the alveolar space (C, C‘ higher magnification). Scale bar: 1 mm (B, C); 500 µm (B‘, C‘).

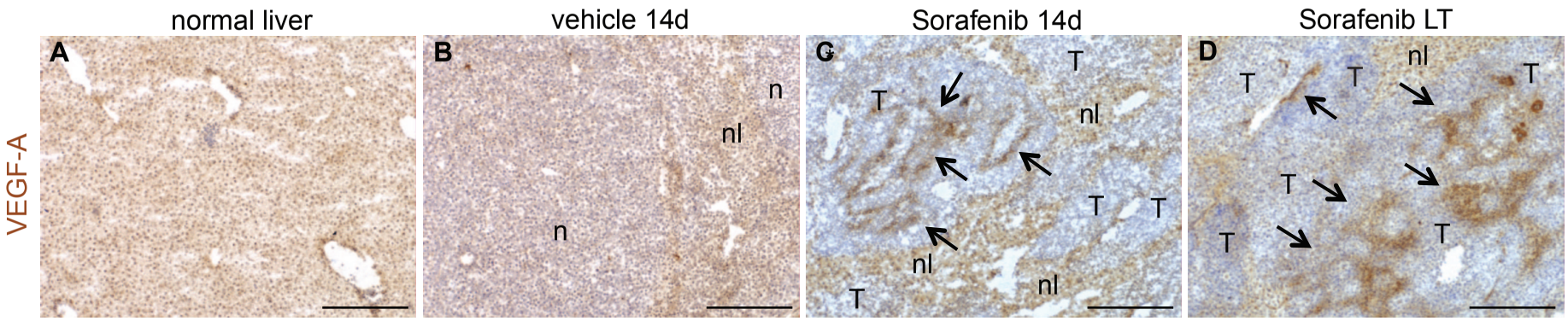

Supplementary Figure S5: VEGF-A expression after Sorafenib treatment. Representative images of VEGF-A staining of frozen liver sections. Normal liver represented a relatively high baseline VEGF-A expression (A). After 14d of vehicle treatment, VEGF-A expression was slightly upregulated within the nodular area (B). After 14d of Sorafenib treatment, VEGF-A expression was upregulated in some nodules (arrows in C), whereas long-term Sorafenib-treated liver samples exhibited extensive VEGF-A upregulation (arrows in D). Scale bar: 500 µm; n, normal liver; T, tumorigenic area; n, nodules.

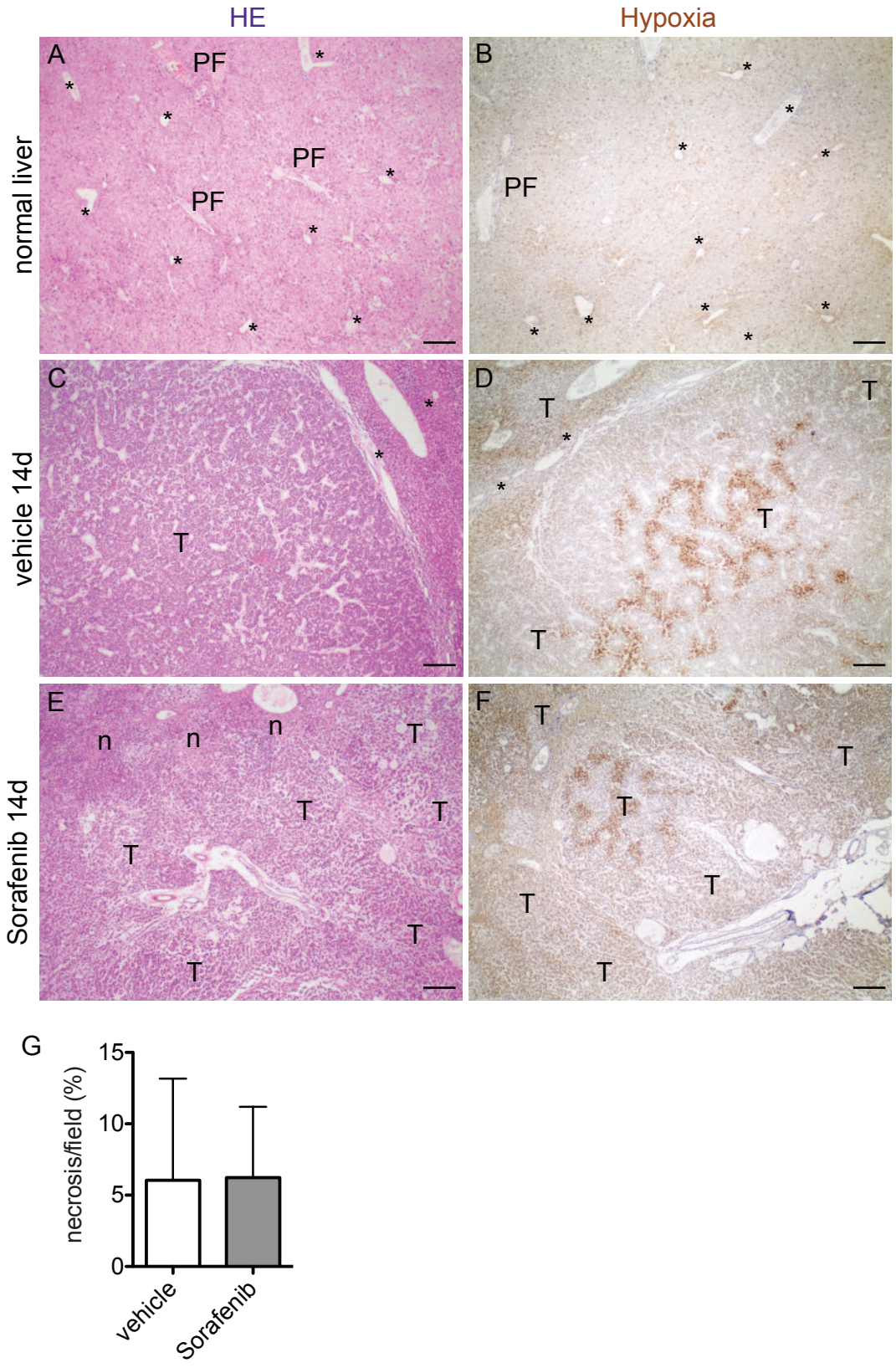

Supplementary Figure S6: Necrosis and hypoxia in Sorafenib-treated iAST mice. HE (A, C, E) and hypoxia (B, D, F) staining of paraffin-embedded liver sections from adenoviral Cre-injected mice of normal (A, B), 14d vehicle- (C, D) and 14d Sorafenib- (E, F) treated animals. Normal liver stained weakly for hypoxia around central veins (*). Liver of 14d vehicle- and Sorafenib-treated iAST mice showed hypoxia-positive stained tumorigenic areas. (G) Quantification of necrotic areas indicated no overall difference comparing vehicle- and Sorafenib-treated animals (N=3 mice per group). Scale bar: 200 µm; PF, portal field; n, necrotic area; T, tumorigenic area.

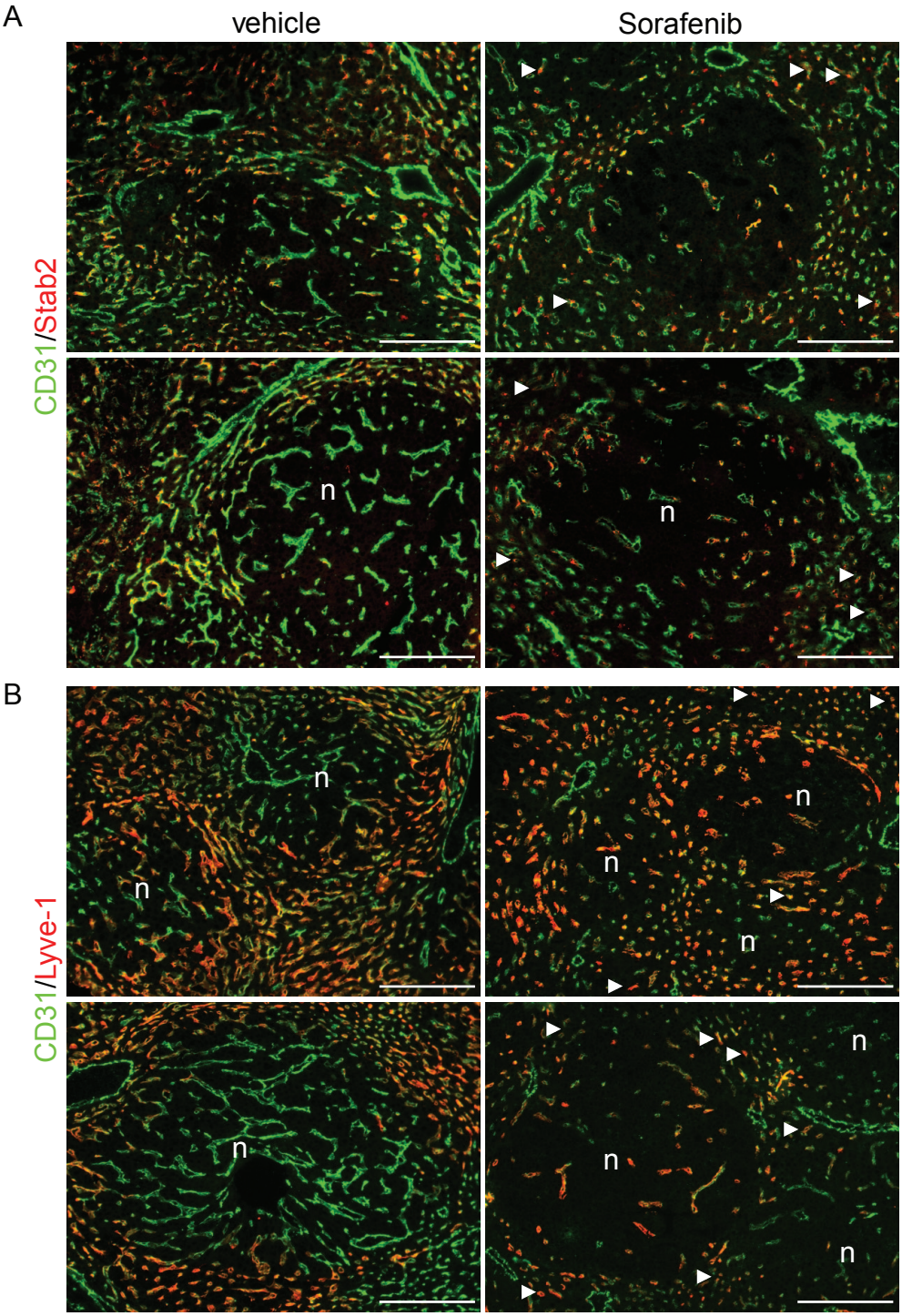

Supplementary Figure S7: Sinusoidal marker expression upon Sorafenib treatment. Representative images of frozen liver sections from iAST tumor-bearing mice 14 days after vehicle and Sorafenib treatment initiation. Double immunofluorescence staining for CD31 (green) and Stabilin-2 (red) (A), and CD31 (green) and Lyve-1 (red) (B), showing sinusoidal marker expression outside the tumor nodule area (arrowheads). Scale bar: 200 µm; n, nodule.

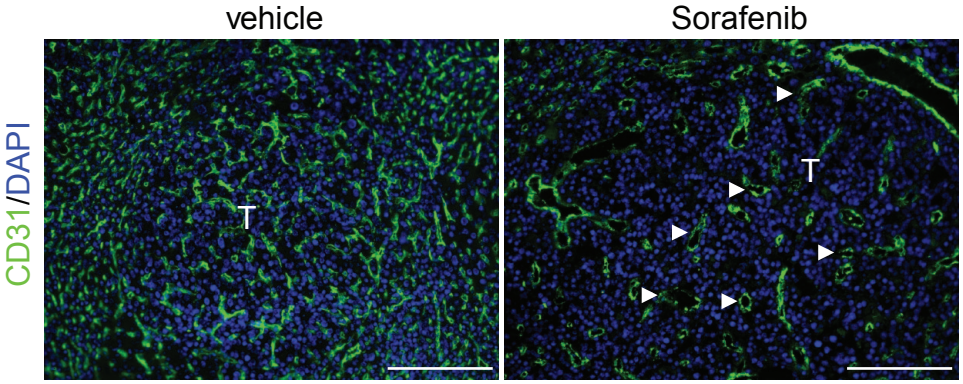

Supplementary Figure S8: Vascular remodeling upon Sorafenib treatment. Representative images of frozen liver sections from iAST mice 14 days after vehicle and Sorafenib treatment initiation. Immunofluorescence staining for CD31 (green) showing increased tumor vessel diameter upon Sorafenib treatment (arrowheads). Nuclei were counterstained with DAPI (blue). Scale bar: 200 µm; T, tumorigenic area.

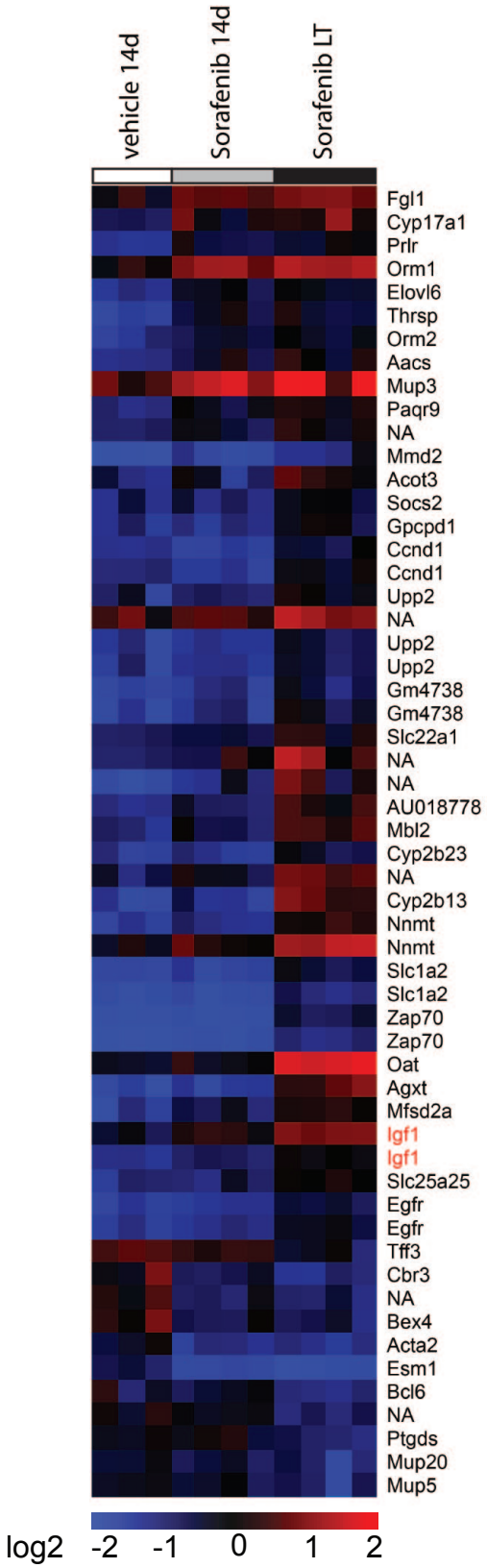

Supplementary Figure S9: Microarray data analysis. Microarray heatmap of the 56 most changed genes of whole liver lysates from 14d vehicle- and Sorafenib-, as well as long-term (LT) Sorafenib-treated mice. Data were analyzed using Chipster software.

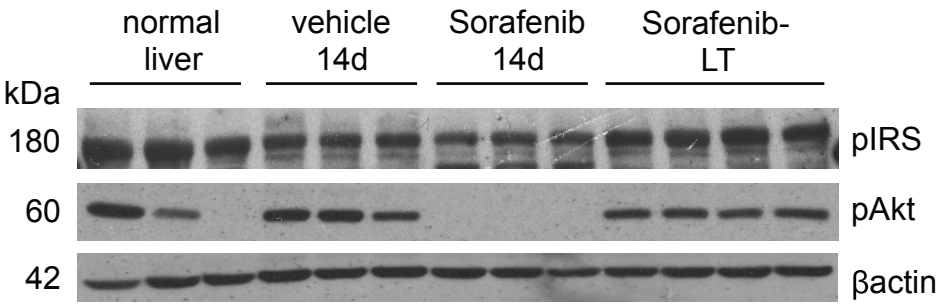

Supplementary Figure S10: Regained proliferative potential after LT-Sorafenib administration. Western blot analysis of activated IRS and Akt of normal-, 14d vehicle-, 14d Sorafenib- and LT-Sorafenib-treated iAST tumor-bearing mice. Activated IRS, substrate of activated IGF-1R, and activated Akt were again upregulated in the LT-Sorafenib-treated animals (N=3-4 mice per group).

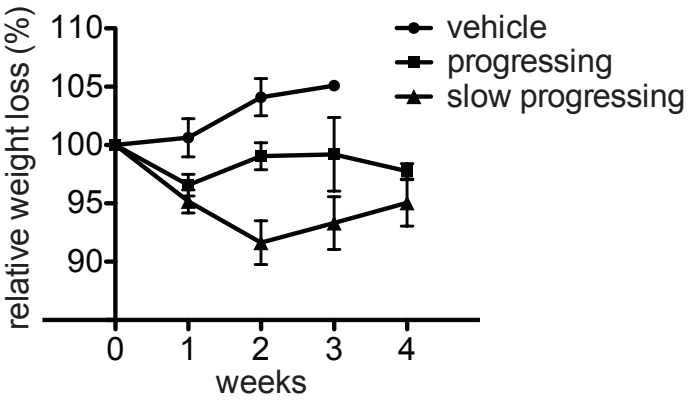

Supplementary Figure S11: Stable weight in Sorafenib-treated iAST mice. Sorafenib-treated (40 mg/kg) and MRI staged mice, were divided in two groups: progressing (end stage) and slow progressing (before end stage). No severe weight loss was observed over the treatment period.

Materials and Methods

Whole mount liver imaging. Small pieces of liver (approx. $1cm^3$) were visualized by whole mount staining with mouse monoclonal anti-human/mouse αSMA directly labeled with Cy3 antibody (1:100; Sigma) using optical projection tomography (OPT) Scanner 3100 (Bioptonics). Staining, imaging, and 3D reconstruction were performed as described previously [1].

Microcast of the liver vasculature. Anesthetized mouse was perfused via the portal vein with EGTA buffer for 5 minutes followed by 120 µl of pre-mixed MICROFIL solution (MV-122, Flow Tech Inc.). Immediately after injection a vessel clip was applied to prevent reflux. After 90 min incubation at room temperature (RT) the whole liver was dissected and subjected to serial dehydration steps according to the manufacture's protocol. Next, the liver was incubated with methyl salicylate (Sigma-Aldrich) for 2 h at RT. Images were taken with the Olympus, X71 microscope.

Vascular analysis. Endothelial cells, pericytes, and basement membrane of blood vessels in tumorigenic livers as well as tumor nodules were quantified by measuring the proportion of sectional area (area density) occupied by fluorescence of specific immunohistochemical markers. Digital fluorescence microscopic images, each representing a region measuring 1376 × 1280 pixels (×10 objective, ×1 Optovar), were captured from sections of at least 5 iAST tumorigenic livers. Five fields per section in vehicle- and Sorafenib-treated animals and at least 10 nodules of different sizes from iAST mice were randomly analyzed. Images were captured with a digital camera attached to an epifluorescent microscope (Olympus, X81). To quantify the co-localization between corresponding image channels (CD31, αSMA, Desmin, or Collagen type IV), we have developed an automated image analysis approach. With this approach, statistical image information such as the maximal image intensity and the mean intensity was computed and based on this information image segmentation was performed using either Otsu thresholding [2] or an adaption of the triangle threshold method [3]. In the former method, an optimal threshold was determined by minimizing the intra-class variances, whereas the latter method exploited information of the shape of the image histogram. The respective method was applied either to the whole image or to each single nodule area separately. Co-localization between different channels was quantified by computing the region overlap as the absolute number of pixels between the segmented regions in the corresponding channels. The branching of the vessel structure was quantified by computing the absolute number of junctions of the topological skeleton of the binary (segmented) image.

The area of CD31-positive objects was quantified as described above. Percentage of microvessel area (MVA, %) in each field was calculated as [(area of CD31-positive objects/measured tissue area or nodule area) x 100%]. Mean values of microvessel area (MVA) in each group were calculated from at least five tumorigenic liver samples of vehicle- and Sorafenib-treated animals. Data were analyzed

with unpaired Student's *t*-test (Prism, version 5). P<0.05 was considered statistically significant. Mean values of MVA in the nodules were calculated from at least 10 nodules per group. Data were analyzed with unpaired Student's *t*-test (Prism, version 5). P<0.05 was considered statistically significant.

Co-localization of pericyte markers and collagen type IV: As an index of pericyte maturation, the amount of co-localization of 2 pericyte markers (αSMA and Desmin) was measured on images of immunohistochemically stained 7-µm sections of iAST tumorigenic livers and liver tumor nodules. Digital images of the red (Cy3-labeled αSMA primary antibody) and green (CD31 labeled with Alexa488-conjugated secondary antibody) or red (Alexa546-labeled secondary antibody for Desmin detection) and green (CD31-labeled with Alexa488-conjugated secondary antibody) channels of the same field were captured separately with a digital camera attached to the epifluorescence microscope (×10 objective). The co-localization in the red and green channel was quantified as described above. Perivascular coverage and collagen IV surrounding vessels were quantified as percentage of the total vessel area.

Non-co-localization of pericyte markers and Collagen type IV: Co-localization of the pericyte channel and the collagen channel was quantified as the absolute number of pixels, which were located within an Euclidean distance of 10 pixels to the segmented collagen regions. Accordingly, the number of not co-localizing pixels was defined as the difference of the number of all segmented pixels of the pericyte channel and the number of co-localizing pixels. Non-covering pericytes and collagen type IV were quantified as percentage of the total pericytes or collagen type IV area.

Microscopes. Fluorescent images were obtained with Olympus, X81; Zeiss, LSM710 and Zeiss, CellObserver. Bright field images were obtained with Olympus, X71 and Olympus, BX53.

Western blot analysis. Liver samples were homogenized in lysis buffer and 100 µg of protein lysates were separated on either 8% or 10% polyacrylamide/SDS gels, blotted on nitrocellulose membranes and incubated with primary antibodies at 4°C over night. The following primary antibodies were used: rabbit anti-phospho-VEGFR2 (1:1000; Invitrogen); rabbit anti-VEGFR2 (1:1000; Cell Signaling Technology), rabbit anti-phospho-PDGFRβ (1:1000; Abcam); rabbit anti-PDGFRβ (1:1000; Cell Signaling Technology), mouse anti-Tie2 (1:1000 Upstate/Millipore), rabbit anti-Ang1 (1:500; BioTrend), rabbit anti-Ang2 (1:500; Calbiochem), rabbit anti-bRaf (1:1000; Cell Signaling Technology), rabbit anti-cRaf (1:1000; Cell Signaling Technology), anti–phospho-Ser^{473}-AKT (1:2000; Cell Signaling), rabbit anti-AKT (1:1000; Cell Signaling), rabbit anti–phospho-Thr^{202}/Tyr^{204}-ERK1/2 (1:1000; Cell Signaling Technology), rabbit anti-phospho-IRS-1 (1:1000; Cell Signaling), mouse anti-ERK1/2 (1:1000; Santa Cruz) and anti-mouse β-actin (1:5000; Santa Cruz). Goat anti-mouse and goat anti-rabbit

horseradish peroxidase (HRP)-conjugated secondary antibodies (1:5000; Dako) were used. Detection of chemiluminescence was done with ECL Western blotting substrate (Pierce).

ELISA. VEGF concentrations were analyzed with the sandwich ELISA kit (R&D Systems) following the manufacturer's protocol. Liver specific VEGF concentration was measured in homogenized liver samples that were adjusted for equal total protein concentration (3.5 mg/ml), and VEGF concentration from serum was measured after diluting the serum according to the manufacturer's instructions. Duplicates of serum and liver lysate samples were determined. IGF1 concentrations were analyzed in duplicates with the ELISA kit (Abcam) following the manufacturer's protocol. Homogenized whole liver lysates were adjusted to total protein concentration (120 µg/ml), and IGF1 serum concentrations were diluted 1:250.

Quantitative RT-PCR (qPCR): Total RNA was isolated from liver samples using the Tri Reagent (Sigma) following the manufacturer's protocol. mRNA (1 or 2 µg) was transcribed into cDNA using the Quantitect Reverse Transcription kit (Qiagen) and diluted 1:10 for qPCR. cDNA (4.5 µl) was used for qPCR using 5 µl Taqman Fast Advanced Master Mix (Applied Biosystems) and 0.5 µl Taqman primer/probe mix (AppliedBiosystems) in a 10 µl reaction on an ABI StepOnePlus cycler (Applied Biosystems) or LightCycler 480 (Roche) was used: *Ang1*, *Ang2*, *Tie2*, *Vegfa*, *Vegfr2*, *αSma*, *Desmin*, *Pdgfrβ*, *Ng2*, *CD248*, *Rgs5*, *Id1*, *Igf1*, *Hgf*, *cMet*, *Hbegf*, *β2 microglobulin* was used as endogenous control in the ΔΔCt analysis.

Microarray analysis. Microarrays were performed by the core facility of the DKFZ in Heidelberg. In brief, total RNA was extracted as described above. The quality and concentration of total RNA was checked by gel analysis using the total RNA Nanochip assay on an Agilent 2100 Bioanalyzer and NanoDrop. The samples were then reverse transcribed into biotin-labeled cDNA and hybridized on Illumina Mouse Sentrix-8 BeadChip arrays (Illumina Inc, Version-2) according the manufacturer's instructions. Microarray data were collected with an iScan array scanner and analyzed using Chipster software.

References

1. Alanentalo T, Asayesh A, Morrison H, Loren CE, Holmberg D, Sharpe J, et al. Tomographic molecular imaging and 3D quantification within adult mouse organs. Nature Methods, 2007; 4:31-3.
2. Otsu, N., 1979. A threshold selection method from gray-level histograms. Systems, Man, and Cybernetics. 1979;9:62-6.
3. Zack GW, Rogers WE, Latt SA. Automatic measurement of sister chromatid exchange frequency. J Histochem Cytochem. 1977;25:741-53